Enhanced resolution in Fourier incoherent single channel holography (FISCH) with reduced optical path difference

Roy Kelner,[1,*] Joseph Rosen,[1,4] and Gary Brooker[2,3,5]

[1]*Department of Electrical and Computer Engineering, Ben-Gurion University of the Negev, P.O. Box 653, Beer-Sheva 8410501, Israel*

[2]*Department of Biomedical Engineering, Johns Hopkins University, 9605 Medical Center Drive, Rockville, Maryland 20850, USA*

[3]*Microscopy Center, Johns Hopkins University Montgomery Country Campus, Rockville, Maryland 20850, USA*

[4]*rosen@ee.bgu.ac.il*

[5]*gbrooker@jhu.edu*

[*]*kelnerr@post.bgu.ac.il*

Abstract: Fourier incoherent single channel holography (FISCH) is a method for recording spatially incoherent digital Fourier holograms. We present a general design of enhanced FISCH with a smaller optical path difference between interfering beams, when compared to our initial design [Opt. Lett. **37**, 3723]. This reduction enables a proper system operation with a wider bandwidth. Potential resolution enhancement of the images reconstructed from the FISCH holograms consequentially follows.

OCIS codes: (090.0090) Holography; (090.1995) Digital holography; (110.6880) Three-dimensional image acquisition; (100.3010) Image reconstruction techniques; (070.6120) Spatial light modulators.

References and links

1. R. Kelner and J. Rosen, "Spatially incoherent single channel digital Fourier holography," Opt. Lett. **37**(17), 3723–3725 (2012).
2. G. Brooker, N. Siegel, V. Wang, and J. Rosen, "Optimal resolution in Fresnel incoherent correlation holographic fluorescence microscopy," Opt. Express **19**(6), 5047–5062 (2011).
3. J. Rosen, N. Siegel, and G. Brooker, "Theoretical and experimental demonstration of resolution beyond the Rayleigh limit by FINCH fluorescence microscopic imaging," Opt. Express **19**(27), 26249–26268 (2011).
4. B. Katz, J. Rosen, R. Kelner, and G. Brooker, "Enhanced resolution and throughput of Fresnel incoherent correlation holography (FINCH) using dual diffractive lenses on a spatial light modulator (SLM)," Opt. Express **20**(8), 9109–9121 (2012).
5. J. Rosen and G. Brooker, "Fresnel incoherent correlation holography (FINCH) – A review of research," Adv. Opt. Technol. **1**, 151–169 (2012).
6. M. K. Kim, "Adaptive optics by incoherent digital holography," Opt. Lett. **37**(13), 2694–2696 (2012).
7. I. Yamaguchi and T. Zhang, "Phase-shifting digital holography," Opt. Lett. **22**(16), 1268–1270 (1997).
8. D. N. Naik, G. Pedrini, and W. Osten, "Recording of incoherent-object hologram as complex spatial coherence function using Sagnac radial shearing interferometer and a Pockels cell," Opt. Express **21**(4), 3990–3995 (2013).
9. O. Bryngdahl and A. Lohmann, "Variable magnification in incoherent holography," Appl. Opt. **9**(1), 231–232 (1970).
10. B. Katz and J. Rosen, "Super-resolution in incoherent optical imaging using synthetic aperture with Fresnel elements," Opt. Express **18**(2), 962–972 (2010).
11. J. W. Goodman, *Introduction to Fourier Optics* (Roberts and Company Publishers, 2005).
12. X. Lai, S. Zeng, X. Lv, J. Yuan, and L. Fu, "Violation of the Lagrange invariant in an optical imaging system," Opt. Lett. **38**(11), 1896–1898 (2013).
13. M. Born and E. Wolf, *Principles of optics* (Cambridge, 1999), Chap. 4.4.5, p. 176.
14. E. Wolf, *Introduction to the Theory of Coherence and Polarization of Light* (Cambridge, 2007).
15. P. Hariharan, *Optical holography principles, techniques, and applications* (Cambridge, 1996), Chap. 15, p. 247 and Chap. 17, p. 296.
16. J. A. Neff, R. A. Athale, and S. H. Lee, "Two-dimensional spatial light modulators: a tutorial," Proc. IEEE **78**(5), 826–855 (1990).
17. G. Pedrini, H. Li, A. Faridian, and W. Osten, "Digital holography of self-luminous objects by using a Mach-Zehnder setup," Opt. Lett. **37**(4), 713–715 (2012).
18. O. Bouchal and Z. Bouchal, "Wide-field common-path incoherent correlation microscopy with a perfect overlapping of interfering beams," J. Europ. Opt. Soc. – Rap. Pub. **8**, 13011 (2013).

#190662 - $15.00 USD Received 16 May 2013; revised 23 Jul 2013; accepted 25 Jul 2013; published 20 Aug 2013

1. Introduction

Fourier incoherent single channel holography (FISCH) is a recently developed method for recording digital Fourier holograms of spatially incoherent scenes [1]. Its development followed the successful realizations of the Fresnel incoherent correlation holography (FINCH) system [2–5], and was inspired by the many advantageous properties of FINCH, which are also inherent in FISCH.

Both FINCH and FISCH are distinctively characterized by their structure of a single channel incoherent interferometer. A single beam of light, emitted from a single point source, is modified using spatial light modulators (SLMs) to split the emitted light into two separate beams. The beams propagate through the interferometer within the same path, until reaching a digital camera, where an interference pattern, representing the point source three-dimensional (3D) location, is formed and recorded. This single channel configuration is fundamentally robust being essentially immune to vibration and is easier to align when compared to classical dual-path holography systems.

Though we deliberately chose to implement both systems in a single channel configuration, the adaptation of their conceptual method of operation into a dual-path form is straight-forward. This has the possible advantage of eliminating the need for an SLM (see, for example [6]), though at the price of losing the single channel advantage. Still, in-line Fresnel holograms suffer from the well-known twin image problem, where a single object results with two conjugated images, commonly referred to as the image and its twin, and an additional 0th diffraction order term. In the hologram reconstruction process, overlapping and inseparable light (i.e., information) that is emitted from the two images, and from the 0th order term, renders the resulting reconstruction unusable, as it appears blurry and noisy. Consequentially, one must find a way to eliminate the twin image and the unwanted 0th order term, usually by applying a phase-shifting procedure [2–7] that requires at least three exposures. This procedure is necessary in FINCH, so even if a SLM is not used in any FINCH dual-path configuration, alternative phase-shifting devices (e.g., phase retarders, piezo mounted mirrors) are still needed. In FISCH, a Fourier hologram is recorded where the three diffraction orders can be angularly separated. Hence, it is possible to eliminate the twin image problem by recording a hologram of a scene that occupies only a half-plane. By the term half-plane, we mean that any straight line crossing the origin divides the plane to two equal halves. The complete 3D information of the scene can therefore be extracted from a single FISCH exposure. In this case, however, a high bias level in the recorded hologram might compromise the quality of the reconstruction results [1].

The introduction of FISCH has recently been followed by another successful attempt of recording spatially incoherent digital Fourier holograms using a radial shearing interferometer [8]. In that work, the recorded Fourier hologram results from the interference of two wavefronts that represent the same single point source object, but with different magnifications of α and $\beta = 1/\alpha$. In our original FISCH design [1], the magnification of the two wavefronts are usually one (α) and minus one (β), giving rise to a potentially higher resolution, but also to an increased optical path difference (OPD). This situation can be compared with a rotational shearing of 180°. However, the interference of two wavefronts that only differ from each other by a pure rotational shearing, as in the case of a rotational shearing interferometer (RSI) [9], results in complete loss of any depth information, whereas in FISCH, interfering beams from points of non-zero depth have different spherical wavefronts, and so depth information is retained.

In this paper, an enhanced FISCH design is introduced, offering reduced OPD, without sacrificing the system resolution. Moreover, due to the OPD reduction, the system can efficiently handle signals of wider bandwidths, with minimal resolution loss, in comparison to our initial design [1], whenever the OPD is a limiting factor. Additionally, the new design is implemented using two SLMs, and therefore offers greater flexibility, such that the FISCH system can be instantaneously transformed into a FINCH system, and vice versa. This is in contrast to our less flexible original FISCH design, in which only a single SLM was

#190662 - $15.00 USD Received 16 May 2013; revised 23 Jul 2013; accepted 25 Jul 2013; published 20 Aug 2013

configured in a double-pass mode [1]. Various characteristics of spatially incoherent holography systems that are mentioned throughout this paper are detailed in Appendix 1.

2. System design and theoretical analysis

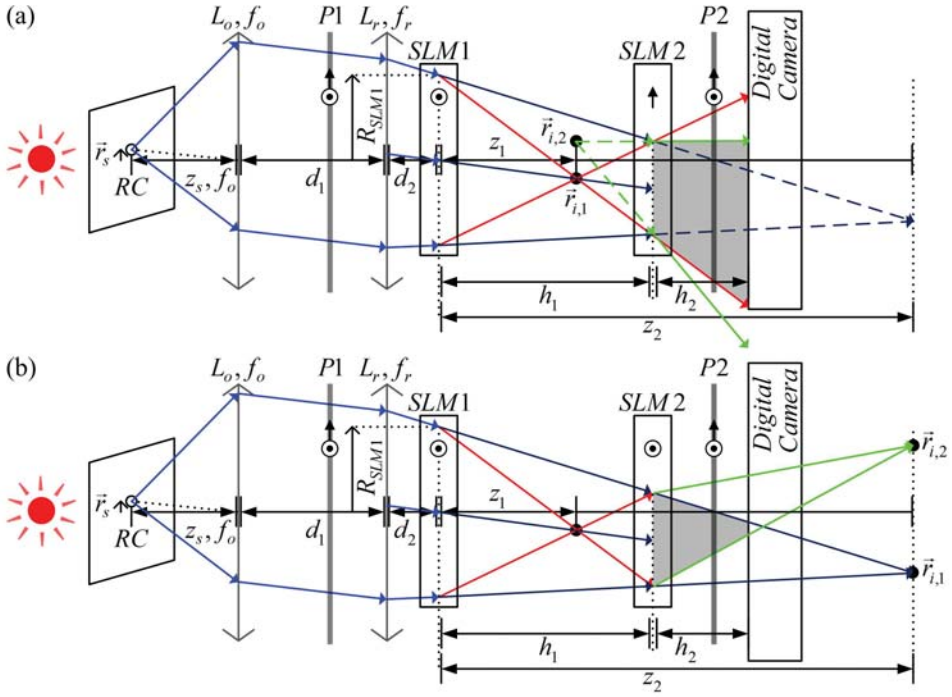

Fig. 1. Schematics of two FISCH recorder designs: *RC*, resolution chart; *SLM*, spatial light modulator; *P*1 and *P*2, polarizers; L_o and L_r, lenses. In (a) the polarization sensitive axes of the SLMs are perpendicular to each other, whereas in (b) they coincide with one another (i.e., in parallel). The symbols ⊙, ↑ and ⦿ are polarization directions parallel, perpendicular and at 45° to the plane of the page, respectively.

Two proposed designs of enhanced FISCH are schematically presented in Fig. 1. The systems consist of a collimation lens L_o, two SLMs located between two, in parallel, polarizers, and a digital camera. An additional refractive lens L_r, which was not used in our earlier FISCH design [1], is located between L_o and the first SLM. We first describe the design shown in Fig. 1(a), and follow with a short discussion of the differences between that system and an alternative design depicted in Fig. 1(b). The SLMs are placed with their active axes perpendicular to each other and at a 45° angle to the transmission axis of the polarizers. Each SLM only modulates the phase-components of the incident light that have their polarization aligned with its active axis, while components of perpendicular polarization, aligned with the non-active axis of the SLM, are not affected [2]. This configuration enables separate control over perpendicular polarization components of the light beam traveling within the system.

The working concept of FISCH is depicted in Fig. 1(a), where a point object is located at the front focal plane of the collimation lens L_o, so that $z_s = f_o$. A diverging spherical wave, induced from the point source, is collimated into a plane wave by the lens L_o, and is converged into a spherical wave by the refractive lens L_r. This wave is eventually transformed into two beam cones: one that diverges from the real image point $\vec{r}_{i,1}$, due to *SLM*1 (with a phase mask forming a converging diffractive lens), and one that diverges from

#190662 - $15.00 USD Received 16 May 2013; revised 23 Jul 2013; accepted 25 Jul 2013; published 20 Aug 2013

the virtual image point $\vec{r}_{i,2}$, due to *SLM*2 (forming a diverging diffractive lens). The focal lengths of the two, SLM-realized, diffractive lenses are determined so that the two image points, $\vec{r}_{i,1}$ and $\vec{r}_{i,2}$, are formed at a distance z_1 from *SLM*1, on the same transverse plane. The two beam cones originate from the same source and are therefore spatially coherent. Their interference results with a cosine fringe pattern on the digital camera, representing the source location $\vec{r}_s = (x_s, y_s)$. If the object point is located outside of the front focal plane of L_o, the two image points are not formed at equal z-distances from *SLM*1, because of different locations and focal lengths of the imaging lenses of the two points (both points share L_o and L_r, but their final image is formed either by *SLM*1 or by *SLM*2). As a result of the longitudinal gap between the image points, a quadratic phase term, representing the point source depth location, z_s, is encoded into the fringe pattern. Fringe patterns of all spatially incoherent point sources are summed over the camera, forming a Fourier hologram. Note that similar to the case of the RSI [9], a Fourier hologram is obtained because one image is 180° rotated compared to the other image. However, unlike the RSI, FISCH can store 3D information, and in this sense FISCH is actually a combination of both rotational and radial interferometers.

An alternative configuration of FISCH is presented in Fig. 1(b), where the active axes of both SLMs are in the same direction, and therefore no longer offer control over separate, perpendicular components of polarizations. Still, the working concept strongly resembles the one of Fig. 1(a), except that the interference now occurs between two converging spherical waves: the first converges into the real image point $\vec{r}_{i,1}$, and is not affected (modulated) by either of the SLMs; the second converges into the real image point $\vec{r}_{i,2}$, after being modulated by the two SLMs. It is easy to show that *SLM*1 is similarly used in both configurations, where it acts as a converging diffractive lens, whereas *SLM*2 acts either as a diverging [Fig. 1(a)] or as a converging [Fig. 1(b)] diffractive lens. The focal length of this lens is the same in both configurations, but with an opposite sign. Additionally, when the distance between *SLM*2 and the camera is kept zero, the two configurations are completely equivalent and the hologram is recorded with a perfect overlap of the two beam cones. This is achieved in practice using a relay system as will be discussed later. Further presented analyses and experiments in this study are based on the configuration presented in Fig. 1(a), although a special case of the general configuration of Fig. 1(b) has already been presented in [1], in which interference occurs between two plane waves, thus effectively the two opposite point images are obtained at infinity.

Our mathematical analysis of FISCH starts from the recorded intensity for an arbitrary point source object of complex amplitude A_s, positioned at the coordinate $(\vec{r}_s, z_s)$. This point source induces an inclined spherical wave of the form of $T(x, y; \vec{r}_s, z_s) = A_s L(-\vec{r}_s / z_s) Q(1/z_s)$ over the plane of the collimation lens L_o, where $L(\vec{s}) = \exp[i2\pi\lambda^{-1}(s_x x + s_y y)]$ and $Q(s) = \exp[i\pi s\lambda^{-1}(x^2 + y^2)]$ are the linear and the quadratic phase functions, respectively, in which λ is defined as the central wavelength. Let $*Q(1/z_d)$ denote a Fresnel propagation of a wave along a distance z_d (mathematically, * denotes a two-dimensional convolution), and $\cdot Q(-1/f_l)$ denote the transmission function of a lens of focal length f_l. The following intensity is recorded over the camera plane:

#190662 - $15.00 USD Received 16 May 2013; revised 23 Jul 2013; accepted 25 Jul 2013; published 20 Aug 2013

$$I(x,y;\vec{r}_s,z_s)=\left|T(x,y;\vec{r}_s,z_s)\cdot Q\left(\frac{-1}{f_o}\right)*Q\left(\frac{1}{d_1}\right)\cdot Q\left(\frac{-1}{f_r}\right)*Q\left(\frac{1}{d_2}\right)\cdot Q\left(\frac{-1}{f_1}\right)*Q\left(\frac{1}{h_1+h_2}\right)\right.$$
$$\left.+T(x,y;\vec{r}_s,z_s)\cdot Q\left(\frac{-1}{f_o}\right)*Q\left(\frac{1}{d_1}\right)\cdot Q\left(\frac{-1}{f_r}\right)*Q\left(\frac{1}{d_2+h_1}\right)\cdot Q\left(\frac{-1}{f_2}\right)*Q\left(\frac{1}{h_2}\right)\right|^2, \quad (1)$$

where f_1 and f_2 are the focal lengths of the diffractive lenses realized by SLM1 and SLM2, respectively. Other parameters in Eq. (1) are clearly defined in Fig. 1(a), and include: f_o and f_r, the focal lengths of the two refractive lenses, L_o and L_r, respectively; the L_o to L_r distance, d_1; L_r to SLM1 distance, d_2; the distance between the two SLMs, h_1; and the effective distance between SLM2 and the digital camera, h_2.

Based on a mathematical justification presented in [10], Eq. (1) can be rewritten in the more compact form of:

$$I(x,y;\vec{r}_s,z_s)=\left|A_s b_1 L\left(-\frac{\vec{r}_e}{z_e}\cdot\frac{f_{e,1}}{f_{e,1}+h_1+h_2}\right)Q\left(\frac{1}{f_{e,1}+h_1+h_2}\right)\right.$$
$$\left.+A_s b_2 L\left(-\frac{\vec{r}_e}{z_e+h_1}\cdot\frac{f_{e,2}}{f_{e,2}+h_2}\right)Q\left(\frac{1}{f_{e,2}+h_2}\right)\right|^2, \quad (2)$$

where b_1 and b_2 are constants, $\vec{r}_e=\vec{r}_s f_{e,o} f_{e,r}/[z_s(f_{e,o}+d_1)]$, $z_e=f_{e,r}+d_2$, $f_{e,o}=z_s f_o/(f_o-z_s)$, $f_{e,r}=f_r(f_{e,o}+d_1)/(f_r-f_{e,o}-d_1)$, $f_{e,1}=f_1 z_e/(f_1-z_e)$, and $f_{e,2}=f_2(z_e+h_1)/(f_2-z_e-h_1)$. For spatially incoherent objects, each point source is only spatially coherent to itself and cannot interfere with other points. As a result, the recorded hologram, $H(x,y)$, is simply a summation over all point source contributions:

$$H(x,y)=\iiint I(x,y;\vec{r}_s,z_s)dx_s dy_s dz_s. \quad (3)$$

The values of f_1 and f_2 are inferred from the special case of a point object located at the front focal plane of the lens L_0, as depicted in Fig. 1(a), which results with $f_{e,1}=-z_1$ and $z_e=d_2-f_r=-z_2$. For this case, it can be easily proved that in order to record a Fourier hologram of optimal resolution, $\vec{r}_{i,1}$ and $\vec{r}_{i,2}$ must reside within the same transverse plane, so that the two quadratic terms in Eq. (2) cancel each other. Additionally, a perfect overlap should exist between the two beam cones on the *SLM*2 plane. These conditions are satisfied with $f_1=h_1 z_2/[2(z_2-h_1)]$ and $f_2=-h_1(z_2-h_1)/(2z_2)$. Moreover, the distance between *SLM*2 and the camera should be kept zero (i.e., $h_2=0$). For $h_2\neq 0$ a Fourier hologram is still formed, but its resolution is diminished since complete overlap between the two interfering beams can no longer be achieved. Under the above conditions, Eq. (2) can easily be reduced to:

$$I(x,y;\vec{r}_s,f_o)=\left(|b_1|^2+|b_2|^2\right)I_s+\left[b_1 b_2^* I_s\cdot L\left(\frac{2f_r\vec{r}_s}{f_o}\cdot\frac{1}{z_2-h_1}\right)+c.c.\right], \quad (4)$$

where $I_s=|A_s|^2$ is the intensity of the point source, and c.c. is the complex conjugate of the left term inside the square brackets. As explained in [1], Eqs. (3) and (4) indicate that the

#190662 - $15.00 USD Received 16 May 2013; revised 23 Jul 2013; accepted 25 Jul 2013; published 20 Aug 2013

recorded hologram is of a Fourier type, and its reconstruction process, using a Fourier transforming lens of focal length f_{rec}, can be formulated as:

$$s(x,y,z_{rec}) = \left(v\left[\frac{1}{\lambda f_{rec}}\right]\mathcal{F}^{-1}\{H(x,y)\}\right) * Q\left(\frac{1}{z_{rec}}\right), \tag{5}$$

where $\mathcal{F}^{-1}$ is the inverse Fourier transform (FT), $v[a]$ is the scaling operator, so that $v[a]f(x) = f(ax)$, and z_{rec} is the reconstruction distance for points outside the front focal plane of L_o (with $z_s \neq f_o$), which is, based on Eqs. (2) and (5), equal to:

$$z_{rec} = \pm\frac{f_{rec}^2(f_{e,2} - f_{e,1} - h_1)}{(f_{e,2} + h_2)(f_{e,1} + h_1 + h_2)}. \tag{6}$$

For a point located at $(\vec{r}_s, z_s = f_o)$, the reconstruction distance is $z_{rec} = 0$, thus the reconstruction is the inverse FT of Eq. (4) (assuming $h_2 = 0$):

$$h(\vec{r}_s) = I_s v\left[\frac{1}{\lambda f_{rec}}\right]\mathcal{F}^{-1}\left\{\left(|b_1|^2 + |b_2|^2\right)P(R_H) + \left[b_1 b_2^* I_s \cdot L\left(\frac{2f_r\vec{r}_s}{f_o}\cdot\frac{1}{z_2 - h_1}\right)P(R_H) + c.c.\right]\right\}, \tag{7}$$

where we assume that the system is only aperture limited by R_{SLM1}, the radius of the beam at SLM1 [Fig. 1(a)], restricting the recorded hologram to a clear disc $P(R_H)$ of radius $R_H = R_{SLM1}(z_2 - h_1)/z_2 = R_{SLM1}(z_2 - h_1)/(f_r - d_2)$. Equation (7) contains three terms that represent the 0th order, the point source image, and its twin. Assuming a proper separation of these three terms (with large enough $|\vec{r}_s|$), or the elimination of the unwanted terms, using a phase-shifting procedure [5], the point source image can be shown to be proportional to [11]:

$$h_F(\vec{r}_s) \propto I_s Jinc\left(\frac{2\pi R_H}{\lambda f_{rec}}\sqrt{(x - M_T x_s)^2 - (y - M_T y_s)^2}\right), \tag{8}$$

where $Jinc(r) = J_1(r)/r$, $J_1(r)$ is the Bessel function of the first kind and of order one, and

$$M_T = \frac{2f_{rec}f_r}{f_o(z_2 - h_1)} \tag{9}$$

is the transverse magnification of the point source, in its reconstruction plane.

In view of a recent publication [12], showing that FINCH violates the Lagrange invariant [13], it is interesting to check how FISCH stands in relation to this general law of imaging systems. The Lagrange invariant actually states that the product of the transverse and angular magnifications is identically one. The transverse magnification is given in Eq. (9) and the angular magnification is $M_A = R_H f_o/(R_o f_{rec})$, where $R_o = R_{SLM1}f_r/(f_r - d_2)$ is the radius of the beam at the refractive lenses. Therefore, the product $|M_A M_T|$ is:

$$|M_A M_T| = \frac{R_H f_o}{R_o f_{rec}}\cdot\frac{2f_{rec}f_r}{f_o(z_2 - h_1)} = 2. \tag{10}$$

Here again FISCH, as FINCH before it, violates the Lagrange invariant. If a perfect overlap between the cones of the two interfering beams is kept, the product of the transverse and angular magnifications is 2 in both FISCH and FINCH. This value of 2 leads to an optimal imaging resolution as is shown next.

#190662 - $15.00 USD Received 16 May 2013; revised 23 Jul 2013; accepted 25 Jul 2013; published 20 Aug 2013

Based on Eq. (8), the width of the system point spread function at the object plane (PSF) is [11]:

$$\Delta = \frac{1.22\lambda f_{rec}}{R_H \cdot M_T} = \frac{0.61\lambda f_o}{R_{SLM1}} \cdot \frac{f_r - d_2}{f_r} = \frac{0.61\lambda f_o}{R_o} = \frac{0.61\lambda}{NA}, \tag{11}$$

where R_o / f_o is the numerical aperture (NA) of the system. Equation (11) indicates that, under the above conditions and assumptions, the introduction of the additional refractive lens L_r into FISCH does not deteriorate the resolution of the system. Comparing the resolution of FISCH that results from Eq. (11) with a conventional imaging system of similar NA, demonstrates the super resolution capability of FISCH. The same capability is exhibited in FINCH and is thoroughly discussed in [3].

In order to record a hologram with adequate fringe visibility, the maximum OPD, δ_{max}, should satisfy the condition:

$$\delta_{max} \le \frac{\lambda^2}{\Delta\lambda}, \tag{12}$$

where $\Delta\lambda$ is the source bandwidth in terms of wavelengths [14]. For points located at the front focal point of the input lens L_o, the maximum OPD is (see Appendix 2 for a detailed description):

$$\delta_{max} = R_{SLM1}^2 \frac{\Delta z}{z_1 z_2}, \tag{13}$$

where $\Delta z = z_2 - z_1$. According to Eq. (13), it is possible to reduce the maximum OPD value, and thereby increase the capabilities of the system, by narrowing the gap Δz. For a fixed h_1 distance between the two SLMs, this is achieved through the introduction of the additional refractive lens, L_r, with a proper selection of its focal length, f_r, where $z_2 = f_r - d_2$. We further note that according to Eq. (13) it is possible to check whether a source of a wide bandwidth violates the maximum OPD condition of Eq. (12). When this condition is violated, the effective R_{SLM1} value [Eq. (11)] might be reduced, below its actual physical dimension (i.e., the radius of SLM1 aperture), thereby decreasing the system resolution.

Obviously, narrowing the gap Δz is limited by a number of practical considerations. Since the length of the holographic grating cycle is directly related to the gap Δz, the pixel size of the camera Δ_p, which records the holographic grating, dictates the lowest limit of Δz. Based on Eq. (7), the length of the hologram grating cycle is $\lambda f_o (z_2 - h_1) / (2 f_r |\vec{r}_s|)$, and this length should not be less than the size of two camera pixels, $2\Delta_p$, in order to guarantee a proper sampling of the hologram. A straight forward calculation indicates that for a given value of $z_2 = f_r - d_2$, the minimal gap Δz is:

$$\Delta z_{\min} = \frac{z_2}{\frac{\lambda f_o z_2}{8\Delta_p |\vec{r}_s|_{\max} f_r} + 0.5}, \tag{14}$$

where $|\vec{r}_s|_{\max}$ is the maximal lateral distance of an object point from the origin. In deriving Eq. (14), we used the relation $h_1 = 2z_1 z_2 / (z_1 + z_2)$, obtained from the condition of perfect overlap between beam cones on SLM2, and the relation $z_1 = f_1 z_2 / (f_1 + z_2)$. It is clear from Eq. (14)

#190662 - $15.00 USD Received 16 May 2013; revised 23 Jul 2013; accepted 25 Jul 2013; published 20 Aug 2013

that in order to satisfy the condition $\Delta z < z_2$ the inequality $\lambda f_o z_2 / (4\Delta_p |\vec{r}_s|_{\max} f_r) > 1$ should be satisfied. In our setup and experiments the values were: $\lambda = 635nm$, $f_r = 100cm$, $f_o = 25cm$, $\Delta_p = 6.5\mu m$, $z_2 = 88cm$, and $|\vec{r}_s|_{\max} \approx 2.3mm$. Therefore, and according to Eq. (14), $\Delta z_{\min} \approx 52.8cm$, which is smaller than the actual $\Delta z \approx 62.1cm$ value used in our experiments.

3. Experiments and results

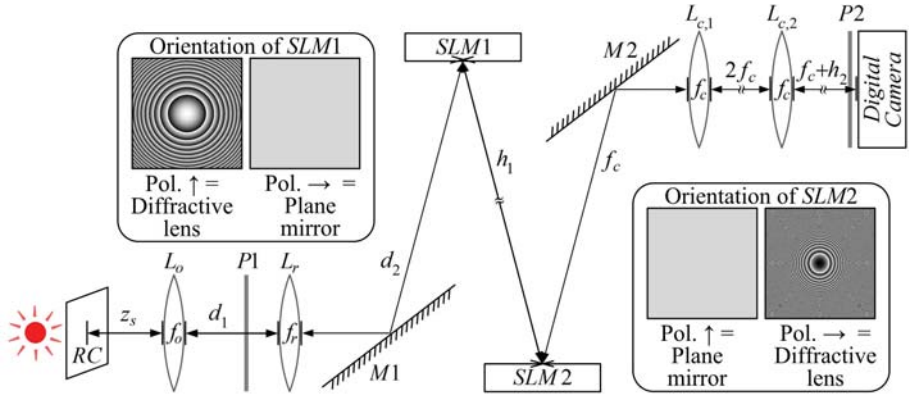

Fig. 2. Experimental setup of FISCH: *RC*, resolution chart; *SLM*1 and *SLM*2, spatial light modulators; *P*1 and *P*2, polarizers; L_o, L_r, $L_{c,1}$ and $L_{c,2}$, lenses; *M*1 and *M*2, mirrors.

The FISCH system we implemented is shown in Fig. 2. This implementation is based on Fig. 1(a), where the active axes of the two SLMs are perpendicular to each other. Additionally, since the SLMs are reflective, a small angle of approximately 7° was introduced between the SLM plane surface normal to the optical axis. The aspect ratios of the phase masks displayed on the SLMs were adjusted to compensate for this angle. Alternatively, the angle could be eliminated by using a beam splitter in front of each SLM [2]. However, this would cause significantly reduced light efficiency. A simple optical relay system of minus one magnification, realized using the 4f system with two refractive lenses, $L_{c,1}$ and $L_{c,2}$ (both with a focal length of $f_c = 15cm$), was inserted between SLM2 and the digital camera to enable choosing any desired effective h_2 values. This addition is required to overcome a technical limitation, where it is physically impossible to place the camera and SLM2 adjacently (see Fig. 2). We used two identical Holoeye PLUTO SLMs (1920x1080 pixels, 8µm pixel pitch, phase only modulation) and a PCO Edge sCMOS camera (2560x2160 pixels, 6.5µm pixel pitch, monochrome). Other parameters in the system were: $f_o = 25cm$, $f_r = 100cm$, $d_1 = 7.5cm$, $d_2 = 12cm$, $h_1 = 40cm$, $f_1 = 36.5cm$, and $f_2 = -10.9cm$.

In the first experiment, two negative NBS 1963A resolution test charts (RCs) served as a target, and were placed simultaneously, using a beam combiner, at two different planes, with $z_{s,1} = f_o = 25cm$ and $z_{s,2} = 27cm$. The effective distance between the second SLM and the camera was set at $h_2 = 4cm$. The charts were back-illuminated using two LEDs (Thorlabs LED631E, $4mW$, $\lambda = 635nm$, $\Delta\lambda = 10nm$). To reduce bias, a two-exposure, real-valued, FISCH hologram was recorded. The two exposures are 180° out of phase from each other, and the final hologram results from their subtraction. As previously noted, a single exposure FISCH hologram is feasible, but two exposures provide better results [1].

The reconstructions of the FISCH recorded holograms are presented in Figs. 3(a)-3(c), clearly demonstrating the refocusing capability of FISCH and its ability to store 3D

#190662 - $15.00 USD Received 16 May 2013; revised 23 Jul 2013; accepted 25 Jul 2013; published 20 Aug 2013

information. Figure 3(a) is the result of a two-dimensional (2D) inverse FT of the recorded hologram, showing both the image of the $z_{s,1} = f_o$ resolution chart and its holographic twin in a sharp focus and with adequate separation, achieved by limiting the RC position to a geometrical half-plane in which the origin (i.e., the optical axis) is not confined. For the second target, located at $z_{s,2} \neq f_o$, the image and its twin no longer reside within the same plane, and additional Fresnel propagation is needed to achieve that plane in focus, as demonstrated in Figs. 3(b) and 3(c). Note that the additional propagation causes de-focusing of the images in the other planes which were previously in focus.

As mentioned in the introduction, the proposed FISCH design can easily be converted into a FINCH system, since two separately controlled SLMs are used. By eliminating the influence of *SLM*2, applying zero phase modulation instead of a quadratic phase function, the system is instantaneously transformed into a dual-lens FINCH system [4], here demonstrated experimentally with a refractive lens (the L_r lens), using the polarization method [2], for the first time. Reconstruction results of the FINCH hologram at two planes of focus are presented in Figs. 3(d) and 3(e). In Figs. 3(f)-3(i), average cross-section curves for the regions marked by a green rectangle in Figs. 3(a), 3(b), 3(d) and 3(e), respectively, are plotted (in blue). These curves are bounded by their upper and lower envelopes (shown in green and red, respectively), from which an estimated visibility curve (in black) was derived. The average value of this curve serves as an estimated visibility (EV) value for the RC lines in the designated regions. Here, EV values of FINCH appear to be somewhat higher than those of FISCH. Additionally, one can observe that the FINCH reconstructions exhibit a higher degree of de-focusing, between different planes of focus. Notice how in Fig. 3(a) one can still observe the figures '18.0' of the out-of-focus RC, whereas in Fig. 3(d) these details are too blurred, and even interrupt with the lower lines of the in-focus 16 line pairs per mm RC.

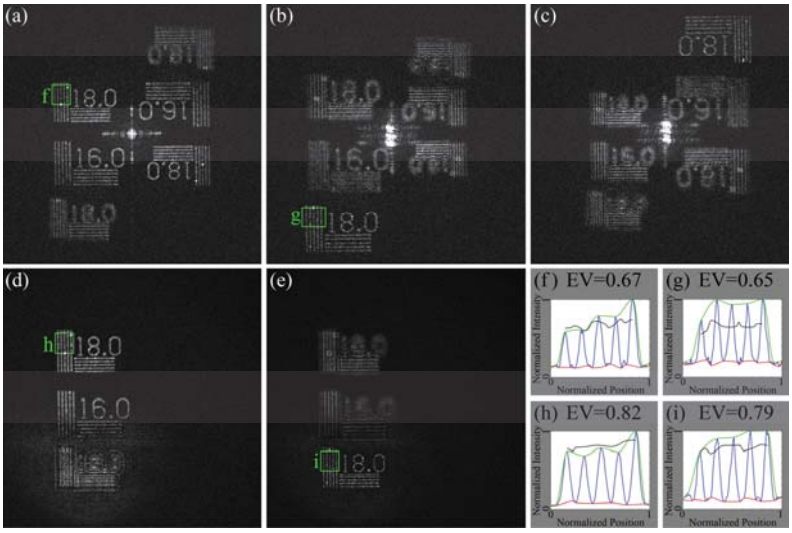

Fig. 3. FISCH reconstructions: (a) top left, at the Fourier plane, where the image of the upper resolution chart (RC) and its twin image are in focus; (b) top center, at the front of the Fourier plane, where only the image of the lower RC is in focus; (c) top right, at the back of the Fourier plane, where only the twin image of the lower RC is in focus. (a) is obtained by a 2D inverse Fourier transform of the final hologram, while (b) and (c) are obtained by a Fresnel propagation from the Fourier plane (a), backward in case of (b), or forward in case of (c). (d), bottom left, and (e), bottom center, are FINCH equivalents of (a) and (b), respectively. The blue curves in (f)-(i), bottom right, represent the average cross-section of the area marked by a green rectangles in (a),(b),(d), and (e), respectively. EV is the estimated visibility value, calculated as the average value of the visibility curve (in black), which was extracted from the upper (green curves) and lower (red curves) envelopes of the average cross section (blue curve).

#190662 - $15.00 USD Received 16 May 2013; revised 23 Jul 2013; accepted 25 Jul 2013; published 20 Aug 2013

To demonstrate the advantages of the suggested FISCH design due to reduced OPD, a second set of experiments was conducted. We used a single NBS 1963A RC as a target, located at $z_s = f_o$, illuminated either with a 10nm full width half max (FWHM) light source (Thorlabs LED631E) or with a 80nm FWHM light source (EKE Halogen lamp, $150W$, followed by a band pass filter of $\lambda = 650nm$, $\Delta\lambda = 80nm$). We tested the system with and without the refractive lens L_r. The focal length f_1 and f_2 were set accordingly, with $f_1 = 36.5cm$ and $f_2 = -10.9cm$ for $f_r = 100cm$ (with L_r), and with $f_1 = -f_2 = h_1 / 2 = 20cm$ for $f_r \to \infty$ (without L_r). All other parameters were left unchanged, except $h_2 = 0$. The ratio between the values of maximal OPD with and without L_r is $2.74/5$, meaning that the maximal OPD value obtained with L_r is almost half of the value obtained without L_r.

The experimental results are presented in Figs. 4(a)-4(d). With $\Delta\lambda = 10nm$ both FISCH configurations demonstrate sufficient resolution to show complete details of the 18 line pairs per mm RC (Figs. 4(a) and 4(c), with EV values of 0.76 and 0.40, respectively). When the illumination is changed to a wider bandwidth, with $\Delta\lambda = 80nm$, both configurations exhibit deterioration of the reconstruction quality (Figs. 4(b) and 4(d)). However, while with $f_r \to \infty$ the lines are smeared into a rectangle (with a low EV value of 0.05), and details are lost, with $f_r = 100cm$, details are preserved and most of the lines are clearly separable (with an EV value of 0.36). This experiment clearly demonstrates the enhanced resolution of the proposed design, due to the reduced OPD as has been previously seen in FINCH [4].

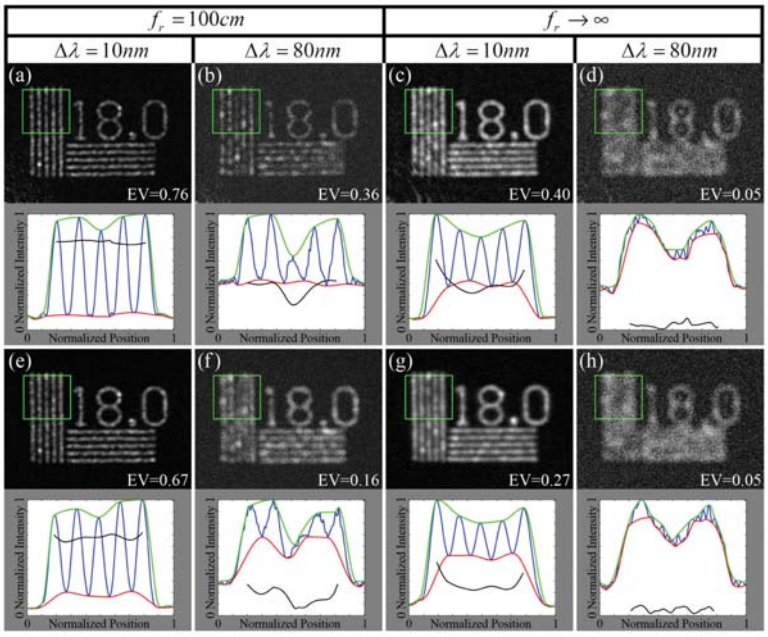

Fig. 4. Effect of bandwidth and OPD on FISCH (a)-(d) and FINCH (e)-(h) resolution: (a),(e) with f_r = 100cm and a 10nm FWHM light source, where all details of the RC are clearly visible; (b),(f) with f_r = 100cm and a 80nm FWHM light source, where the reconstruction quality is diminished, but most details of the RC are still visible; (c),(g) with $f_r \to \infty$ and a 10nm FWHM light source, where most details of the RC are clearly visible but less clear than (a),(e); (d),(h) with $f_r \to \infty$ and a 80nm FWHM light source, where most details of the RC are lost. The blue curve in each sub-figure represents the average cross-section of the area marked by a green rectangle. EV is the estimated visibility value, calculated as the average value of the visibility curve (in black), which was extracted from the upper (green curves) and lower (red curves) envelopes of the average cross section (blue curve). Reconstruction results are shown to match in size.

#190662 - $15.00 USD Received 16 May 2013; revised 23 Jul 2013; accepted 25 Jul 2013; published 20 Aug 2013

We repeated the above experiment with the system transformed into FINCH. Results are presented in Figs. 4(e)-4(h), and demonstrate the same effect of bandwidth and OPD with FINCH as seen in Figs. 4(a)-4(d) for FISCH. Here, also, these observations are further supported by the calculated EV values. We note that the reconstructions presented in Fig. 4 are shown to match in size, to allow easy comparison. Rescaling of the displayed results, where necessary, was achieved by zero-padding the data before the final inverse FT of the reconstruction process had been applied.

4. Summary and conclusions

Two enhanced FISCH configurations have been presented. We have analytically shown that the enhanced FISCH design offers a reduced optical path difference between interfering beams of light. This reduction is achieved without compromising the system resolution. We experimentally demonstrated the enhanced resolution using the proposed system, and also showed that it is superior to our initial design [1] in the sense of operating properly with a wider range of source bandwidth values. These are attributed mainly to the reduced OPD, but may also result from the ability to condense more light (i.e., transfer more information) through the SLMs with our new design. It should also be noted that the best resolution was obtained at shorter bandwidths. This may not be related to the inherent properties of FISCH or FINCH alone, but also due to the fact that the optics and SLMs used in these experiments are not achromatic.

Another interesting observations should be discussed in view of a recently published paper [12] in which it has been indicated that self-interference holography systems violate the Lagrange invariant (also known as the Smith-Helmholtz invariant [13]), in the sense that the product between the transverse (M_T) and the angular (M_A) magnifications is not necessarily equal to 1, as is the case of the entirety of conventional imaging systems. We would like to make the following comments:

1. It is evident from Eq. (10) that FISCH also violates the Lagrange invariant, exactly as happens with FINCH. However, because FISCH with a single exposure can, in principle, produce an output image in real-time using a real-time holographic recorder (e.g., photorefractive crystals, photothermoplastic devices [15], optical-addressed SLM [16]), FISCH can violate the Lagrange invariant in real-time.

2. Not all self-interference holography systems violate the Lagrange invariant. For instance, the system in [17] does not violate the Lagrange invariant, although it is a self-interference holography system. The additional condition which must be satisfied in order to violate the Lagrange invariant is that, for all object points, both object and reference beams should contain information about the location of the same object point.

3. The violation of the Lagrange invariant can be bi-directional, expressed by two inequalities: (a) $1<|M_T M_A|\leq 2$; (b) $0<|M_T M_A|<1$. Only condition (a) is connected to image resolution improvement beyond the classical criterions (i.e., Rayleigh and Abbe resolution criterions). The condition of (b) is fulfilled in the system proposed in [8], for instance. The optimal condition, in terms of best resolution, is obtained when the condition $|M_T M_A|=2$ is satisfied. This last condition is fulfilled in both FINCH and FISCH if and only if there is a perfect overlap between the two beam cones on the plane of the digital camera.

Recently, it was suggested to eliminate the distance between the objective lens and the SLM in FINCH, in order to increase the field of view in the optical system and maintain (or improve) beam centricity around the optical axis [18]. This is achieved using a relay optical system, and can also be applied to the suggested FISCH design using two relay systems for achieving effective zero values of d_1 and d_2. Alternatively, one can use a single relay

#190662 - $15.00 USD Received 16 May 2013; revised 23 Jul 2013; accepted 25 Jul 2013; published 20 Aug 2013

system, and replace the two lenses, L_o and L_r, with one equivalent lens. We hope to realize one of the alternatives in the near future.

The proposed FISCH system can electronically be switched into a FINCH system, without any mechanical intervention, and thus offers the ability to record both Fourier and Fresnel holograms. Note that adding a beam splitter before SLM2 and using two cameras for each channel, enable recording the FINCH and FISCH simultaneously. Consequently, it is possible to exploit any unique advantages of both systems.

Appendix 1

A detailed comparison between spatially incoherent holography systems that were mentioned in this paper is shown in Table 1.

Table 1. Characteristics of Various Spatially Incoherent Holography Systems

Holographic method	Type	Number of exposures[a]	Depth information	Resolution beyond Rayleigh criterion	Configuration	Phase-shifting, method
FISCH[b] [1]	Fourier	One, two, or three	Maintained	Capable	Single channel	Optional, SLM
FINCH [2–5]	Fresnel	Three	Maintained	Capable	Single channel	Required, SLM
Incoherent Digital Holography (IDH)[c] [6]	Fresnel	Four	Maintained	Capable	Dual-path, Michelson interferometer	Required, piezo mounted mirror
Sagnac radial shearing interferometer [8,9]	Fourier	One [9] or five [8]	Maintained	Incapable	Common-path, Sagnac	Optional, Pockels cell [8]
Rotational shearing interferometry (RSI) [9]	Fourier	One	Lost	Capable	Dual-path, Mach-Zehnder	Optional
Holography using a Mach-Zehnder setup [17]	Fresnel	Not stated, presumably three.	Maintained	Incapable	Dual-path, Mach-Zehnder	Required, piezo mounted mirror

[a]Fresnel type holograms require at least three exposures for twin-image removal via phase-shifting, but sometimes more are used. Fourier type holograms may require only a single exposure.
[b]In order to reduce the maximal OPD without sacrificing resolution, two SLMs must be used, instead of one.
[c]IDH is conceptually based on FINCH [6].

Appendix 2

In this appendix an expression of the maximal OPD value as is given in Eq. (13) is derived. We consider the case of a point source object located at the front focal plane of the collimating lens L_o, with $z_s = f_o$, as described in Fig. 5. Without loss of generality, we assume $x_s = 0$ so that $\vec{r}_s = (0, y_s)$. Our OPD analysis follows the assumption that the OPD between an arbitrary pair of points that lie inside the same spherical wavefront of the converging spherical wave exiting the refractive lens L_r is zero (the OPD between point C and point F in Fig. 5, connected by a dashed line that represents the wavefront), so that $\overline{CA} = \overline{FA}$, where $A = (0, -y_i, z_2)$.

#190662 - $15.00 USD Received 16 May 2013; revised 23 Jul 2013; accepted 25 Jul 2013; published 20 Aug 2013

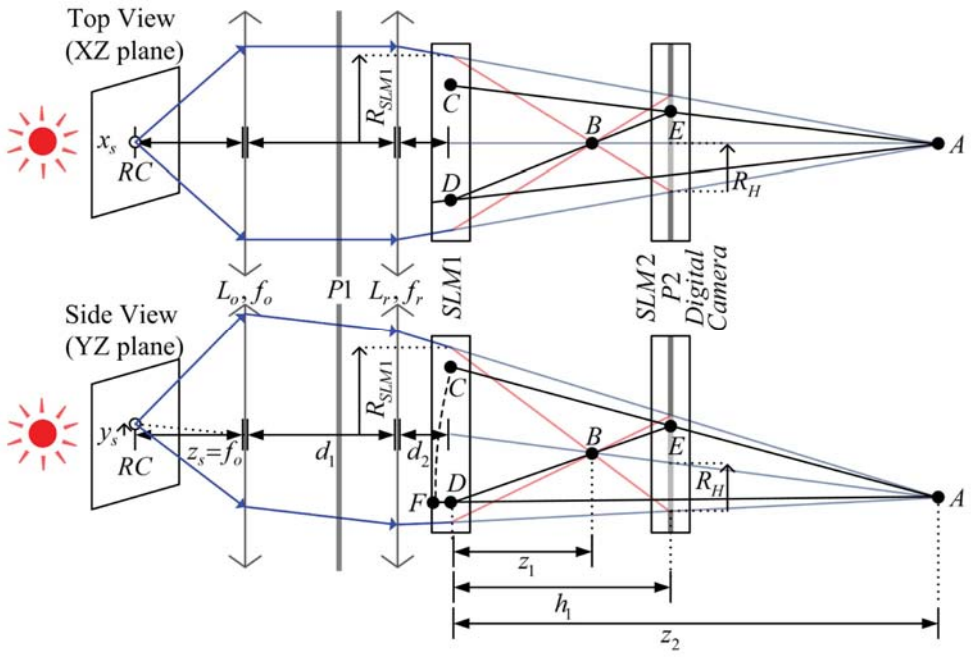

Fig. 5. Schematic of FISCH for finding the OPD at point E in the hologram plane due to a single point source object located at the front focal plane of L_o.

Geometrically, the OPD at an arbitrary point in the hologram plane, $E=(x_H, y_H, h_1)$, is:

$$\delta = \left|\overline{CE} - \overline{FD} - \overline{DE}\right| = \left|\overline{DA} - \overline{DE} - \overline{EA}\right|, \tag{15}$$

where we have used the relations $\overline{CE} = \overline{CA} - \overline{EA}$ and $\overline{FD} = \overline{CA} - \overline{DA}$. Based on triangles similarities, it is easy to show that:

$$\begin{aligned} &B = (0, -y_i z_1 / z_2, z_1),\ C = (x_H z_2 / [z_2 - h_1], -y_i + [y_H + y_i] z_2 / [z_2 - h_1], 0), \\ &D = (-x_H z_1 / [h_1 - z_1], y_H - [y_H + y_i z_1 / z_2] h_1 / [h_1 - z_1], 0), \end{aligned} \tag{16}$$

so that:

$$\begin{aligned} \overline{DA} &= \sqrt{\left(\frac{z_1}{h_1 - z_1}\right)^2 x_H^2 + \left[y_H + y_i - \frac{h_1}{h_1 - z_1}\left(y_H + y_i \frac{z_1}{z_2}\right)\right]^2 + z_2^2}, \\ \overline{DE} &= \sqrt{\left(\frac{h_1}{h_1 - z_1}\right)^2 x_H^2 + \left(\frac{h_1}{h_1 - z_1}\right)^2 \left(y_H + y_i \frac{z_1}{z_2}\right)^2 + h_1^2}, \\ \overline{EA} &= \sqrt{x_H^2 + \left(y_H + y_i\right)^2 + \left(z_2 - h_1\right)^2}. \end{aligned} \tag{17}$$

Under the paraxial approximation we get:

#190662 - $15.00 USD Received 16 May 2013; revised 23 Jul 2013; accepted 25 Jul 2013; published 20 Aug 2013

$$\overline{DA} \approx z_2 \left\{ \frac{1}{2}\left[\frac{z_1}{z_2\left(h_1 - z_1\right)} \right]^2 x_H^2 + \frac{1}{2z_2^2}\left[y_H + y_i - \frac{h_1}{h_1 - z_1}\left(y_H + y_i \frac{z_1}{z_2} \right) \right]^2 + 1 \right\},$$

$$\overline{DE} \approx h_1 \left[\frac{x_H^2}{2\left(h_1 - z_1\right)^2} + \frac{1}{2\left(h_1 - z_1\right)^2}\left(y_H + y_i \frac{z_1}{z_2} \right)^2 + 1 \right], \tag{18}$$

$$\overline{EA} \approx \left(z_2 - h_1\right) \left[\frac{x_H^2}{2\left(z_2 - h_1\right)^2} + \frac{\left(y_H + y_i\right)^2}{2\left(z_2 - h_1\right)^2} + 1 \right],$$

By applying the approximations in Eq. (18) into Eq. (15), together with $h_1 = 2z_1 z_2 / (z_1 + z_2)$, which results from the perfect overlap condition of the two beam cones, and assigning $y_h \triangleq y'_h - 2y_i z_1 / (z_2 + z_1)$ we get:

$$\delta = \left(y'^2_H + x_H^2 \right) \frac{\left(z_2 + z_1\right)^2}{z_1 z_2 (z_2 - z_1)}. \tag{19}$$

The maximal possible value of the $(y'^2_H + x_H^2)$ term in Eq. (19) is equal to R_H^2, the square value of the recorded hologram radius (for a point source), so that:

$$\max\left\{ y'^2_H + x_H^2 \right\} = R_H^2 = R_{SLM1}^2 \frac{\left(z_2 - z_1\right)^2}{\left(z_2 + z_1\right)^2}, \tag{20}$$

where we have used the relation $R_H = R_{SLM1}(z_2 - h_1)/z_2 = R_{SLM1}(z_2 - z_1)/(z_2 + z_1)$. Based on Eqs. (19) and (20) we conclude that the maximal OPD value is:

$$\delta_{max} = R_{SLM1}^2 \frac{\Delta z}{z_1 z_2}, \tag{21}$$

where $\Delta z = z_2 - z_1$.

Acknowledgments

This work was supported by The Israel Ministry of Science and Technology (MOST), by The Israel Science Foundation (ISF) to RK and JR, by NIST ARRA Award No. 60NANB10D008 to GB, and by CellOptic, Inc.

#190662 - $15.00 USD Received 16 May 2013; revised 23 Jul 2013; accepted 25 Jul 2013; published 20 Aug 2013